Soft Matter

Measuring interfacial strength of ultra-soft materials with needle-induced cavitation

Journal:	*Soft Matter*
Manuscript ID	SM-ART-10-2024-001203.R1
Article Type:	Paper
Date Submitted by the Author:	31-Dec-2024
Complete List of Authors:	Fu, Hongbo; University of Massachusetts Amherst, Polymer Science and Engineering Crosby, Alfred; University of Massachusetts, Polymer Science and Engineering

ARTICLE

Received 00th January 20xx,

Accepted 00th January 20xx

DOI: 10.1039/x0xx00000x

Measuring interfacial strength of ultra-soft materials with needle-induced cavitation

Hongbo Fu, [a] Alfred J. Crosby *[a]

Needle-induced cavitation (NIC) has been used to characterize the mechanical properties of ultra-soft biological tissues. Previous studies conducted NIC on brain tissue and computed the energy to separate, or fracture, interfaces between regions from the measured NIC critical pressure. These tests revealed the intrinsic correlation between the critical pressure and the interfacial properties. While NIC demonstrated its potential for measuring interfacial properties, independent measurements have not been made to validate the measurements. In this work, we use model interfaces to validate the use of NIC to quantify the interfacial energy of buried interfaces. By inserting a needle into the interface and inducing pressurized separation, we obtained the critical pressure dependence on the needle size and a known residual stress. At the extrapolated residual stress-free state, we obtained the interfacial energy (G_c) by considering energy dissipated in the separation initiation at the critical pressure point, yielding a G_c value that matches an independent measurement.

1 Introduction

Needle-induced cavitation (NIC) has been extensively studied over the past decade[1–6]. NIC is implemented by applying pressure at a precisely positioned needle tip, forming a cavity, and collecting the pressure profile. The mechanical properties of the specimen can then be determined from the maximum pressure in the pressure profile. NIC has been proven to be effective in determining the modulus of ultra-soft materials, such as biological tissues, at specified locations. Concurrently, NIC has shown the potential to characterize surface and interfacial properties.[7–9] The characterization of the interfacial properties of tissues holds great importance because they contribute to the structural resilience of tissues under deformation;[10] provide insights into disease pathology and dysfunction;[11,12] support biomechanical modelling;[13] guide the selection of autogenous/ extracorporeal biomaterials for reconstructive clinical applications;[12,14,15] and direct pharmacological interventions[16]. Recently, Dougan et al. conducted a study utilizing NIC to evaluate the interfacial energy of brain tissues in vivo[17]. In this method, cavitation was induced by applying hydraulic pressure within the brain tissue, resulting in localized deformation and subsequent rupture around the needle tip. During the test, the pressure profile was collected, and reasonable fractural energy values were computed using hydraulic fracturing models (Figure 1(a)). However, the obtained fracture energy value could not be validated with independent conventional test methods. These methods, such as peel test and tack test, are difficult, if not impossible, to implement for ultra-soft tissues.

To validate the use of NIC at interfaces, in this work we test a specifically designed ultra-soft interface with NIC and demonstrate that the critical pressure can be used to determine the interfacial critical strain energy release rate, G_c, a measure of interfacial strength. We denote this method as "interface-NIC".

We demonstrate the robustness of this method by measuring G_c for interfaces that exist within a bulk material that have different states of residual stress in the as-formed interface. Residual stress, referring to the pre-existing stress within materials before the application of external loads in the bulk, is a crucial factor influencing the performance of various materials. For biological tissues, residual stress can be caused by body forces; thermal expansion or shrinkage; displacement constraints; swelling/deswelling; and tissue growth[18–20]. G_c is a material property; therefore, an accurate measurement of G_c must be devoid of the influence of residual stresses. To investigate the residual stress effect on ultra-soft interfaces, we developed a hydrogel-hydrogel interface by having two surfaces spontaneously contact in a controlled manner. The two hydrogel surfaces were made by placing an inert plastic sheet into the hydrogel precursor solution prior to curing. After curing the hydrogel, this sheet was removed. For sheets thinner than a critical thickness, the hydrogel surfaces that were formed by removing the sheet spontaneously collapse to minimize the system energy, as discussed in a recent publication from our research group.[21] The thickness (t) of the sheet, which defines the initial separation distance between the hydrogel surfaces before collapsing to form an interface (Figure 1(b)), defines the magnitude of the residual normal stress on the closed interface. In this project, we apply needle-induced cavitation at the closed hydrogel interfaces to quantify the influence of residual stress

[a] Polymer Science & Engineering Department, University of Massachusetts Amherst, Amherst, MA 01003, USA. E-mail: acrosby@umass.edu

Electronic Supplementary Information (ESI) available: [details of any supplementary information available should be included here]. See DOI: 10.1039/x0xx00000x

on the critical pressures to open the interface. We develop and validate a relationship between this critical pressure and the G_c for the interface. Thus, these experiments provide important baseline validation for using NIC to characterize the strength, or G_c, of interfaces, both synthetic and natural.

Importantly, due to the interface formation process employed in this study, the geometry of the cavity that develops upon reaching a critical pressure is well-defined as an inflated cylinder at the needle tip. This geometry enables us to derive the pressure-deformation relationship, considering the strain and potential energy during interface opening. Thus, we establish the expression of G_c with the critical deformation (calculated from the critical pressure) and the original undeformed crack size (equivalent to the needle's outer radius). Through the comparison of G_c measured from an independent method, we validate G_c from interface-NIC.

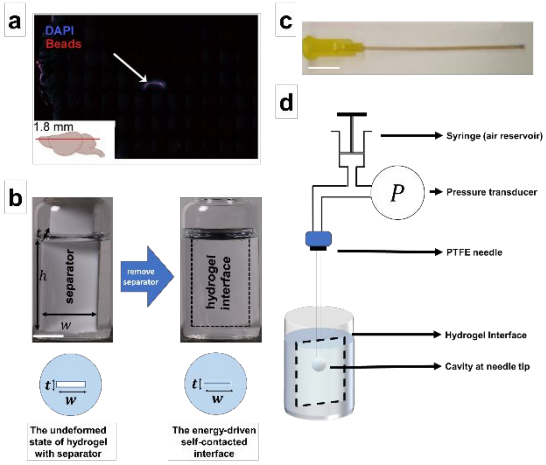

Figure 1. Needle-induced cavitation for ultra-soft interfaces. (a) An interface in brain tissue is opened by NIC. The picture is from reference [17]. Permission to reprint is granted by the publisher. (b) The front view photos and top view schematics of the formation of a self-contacted interface. Scale bar: 1cm (c) A picture of a blunt PTFE dispersing needle. The needle outer diameter is 1.14mm. Scale bar: 1cm. (d) A schematic of the experiment setup for the interface-NIC test.

2 Experiment

2.1. Materials and sample preparation

The monomer acrylamide (AM), crosslinker N,N'-Methylenebisacrylamide (bis-AM), initiator ammonium persulfate (APS), and catalyst tetramethylethylenediamine (TEMED) were purchased from Sigma-Aldrich and used without processing unless otherwise mentioned. PTFE sheets, which are used to create the self-contacting hydrogel interfaces, were purchased from McMaster-Carr and cut into rectangular prisms with a fixed width of 15 mm and length of 52 mm. The plastic needles made of PTFE with different outer radii were purchased from McMaster-Carr and used as received. The PTFE needles are blunt, without sharp edges, as shown in Figure 1(c).

The precursor solution of PAM hydrogel had a weight concentration of 5 wt.%, and the weight ratio of AM to bis-AM was 100:1. We transferred the precursor solution with a volume of 18 mL into a glass vial and added 150 µL of 10 wt.% APS aqueous solution and 15 µL of TEMED under magnetic stirring to initiate hydrogel curing. After 30 seconds of stirring, we removed the stir bar, inserted the PTFE sheet into the solution, and initiated curing. When the hydrogel was fully cured after reacting overnight, we removed the PTFE sheet, releasing the two surfaces, and allowing them to contact to form an interface due to an elasto-adhesion-driven evolution of configuration[21]. The normal residual stress at the interface, denoted as σ_{re}, developed from the deformation of the hydrogel to form the interface. The magnitude of the residual stress is controlled by the thickness of the PTFE sheet, which sets the initial configuration of the hydrogel surfaces prior to interface formation.

2.2. Characterization

2.2.1 Interface-NIC

A pressurization system was used to conduct interface-NIC. A needle is attached to the mobile arm of the Texture Analyzer (model name: TA-AT plus, Micro Stable Systems) to control the displacement. In the tests, the needle is inserted at a depth of 10 mm under the hydrogel surface. We placed the vials containing the hydrogels on the Texture Analyzer's sample stage and positioned the needle tip at the center of the interface, which is formed upon removing the PTFE sheet. When the needle was actuated downward by the mobile arm of the Texture Analyzer, the needle was inserted within the interface. A syringe with a volume of 20 mL was connected to the needle with tubes to introduce positive pressure at the needle tip by compressing the air in the syringe, and the pressure history was monitored with a pressure transducer (model number: PX409-USBH-459210, from OMEGA). A schematic of the experiment setup is shown in Figure 1(d). The compression rate is set at 100 µL/min unless otherwise mentioned.

2.2.2 Indentation method

We applied micro-indentation to measure the hydrogel elastic moduli. A flat steel probe with a radius of 1 mm (part name: TA-52, from Micro Stable Systems) was actuated with a Texture Analyzer to contact the hydrogel from the top, during which we collected the displacement and resultant force of the probe. We calculated the hydrogel modulus based on developed algorithms.[22–24] Detailed information on hydrogel modulus testing is provided in Supplementary S1, and the shear moduli of hydrogel samples are shown in Table S1.

2.2.3 Finite element modelling

To obtain the normal stress at the interface based on the displaced hydrogel surfaces, we developed a two-dimensional plane strain model by using finite element analysis. We considered conditions where the insertion depth of the PTFE sheet far exceeded the PTFE sheet thickness. The model includes a solid circle and a rectangular void, and a schematic is shown in Figure 2(a). The geometric parameters, including the radius of the solid circle, the rectangular void width, and the thickness, were modelled to be the same as the experiment condition. The neo-Hookean model was applied, and we set Young's modulus to be 1 kPa and Poisson's ratio to be 0.495 by setting parameters C10 to be 0.166 and D1 to be 0.066. The

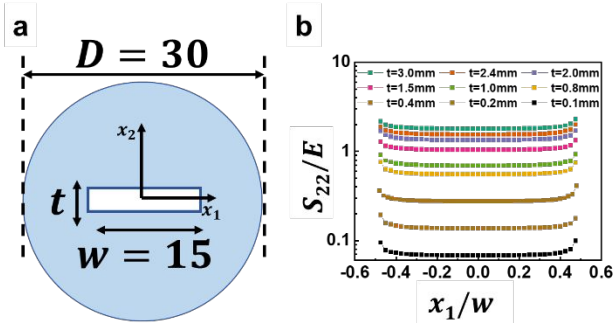

Figure 2. The finite element modeling. (a) The geometry parameters of the solid circle with a rectangular void. Unit: mm (b) The normal stress, S_{22}, distribution as a function of position, x_1, for different initial void thicknesses, t. The values of S_{22} are normalized by the elastic modulus, E, and the position values are normalized by the void width, w. The normal stress approaches a constant value at the interface center, so the normal stress value at $x_1/w = 0$ is chosen to compare with $\Delta P/E$ at the same t.

closed interface configuration was manipulated by applying displacement boundary conditions to the two surfaces with a displacement valued equal to half of the separator thickness. We collected the normal stress perpendicular to the interface from the nodes along the width in the deformed state, as shown in Figure 2(b). Detailed information on FEM is discussed in Supplementary S2.

3. Results and discussion

3.1 Representative interface-NIC test

Figure 3(a) depicts a representative pressure history of an interface-NIC pressurization experiment. As the air in the syringe reservoir is compressed at a constant rate, the pressure at the needle tip increases. The interface at the needle tip remains closed (Figure 3(a) Image (1) and (2)) until a critical point is reached, when the pressure reaches a maximum, denoted as P_c (Image (3)). Upon reaching the maximum pressure, an instantaneous pressure drop occurs, and the interface at the needle tip opens along the plane of the interface (Image (4)).

3.2 Cyclic interface-NIC profile

As the interface is formed by self-contacting surfaces subsequent to hydrogel curing, the interface formation and separation is reversible. To demonstrate the reversibility, we conducted cyclical interface-NIC experiments. The consistent critical pressures measured in these cyclic experiments illustrate the reversibility of the hydrogel interface formation and separation, as shown in Figure 3(b). It is worth noting that Images of Figure 3(b) show an irregular shape of cavities. This is because the exact cavitation happens between two frames of the 30-fps video, and the selected images show the first frame of the post-cavitation time point. Nevertheless, the reversibility of the interface is observed, implying that the failure mechanism associated with the maximum pressure is confined to interfacial failure and does not extend into the hydrogel bulk. Based on the abovementioned findings, we conclude that the soft interface can be opened under pneumatic pressure around the inserted needle tip, and the maximum pressure in the pressure history is correlated with the interface opening. The critical pressure serves as an indicator of interfacial strength.

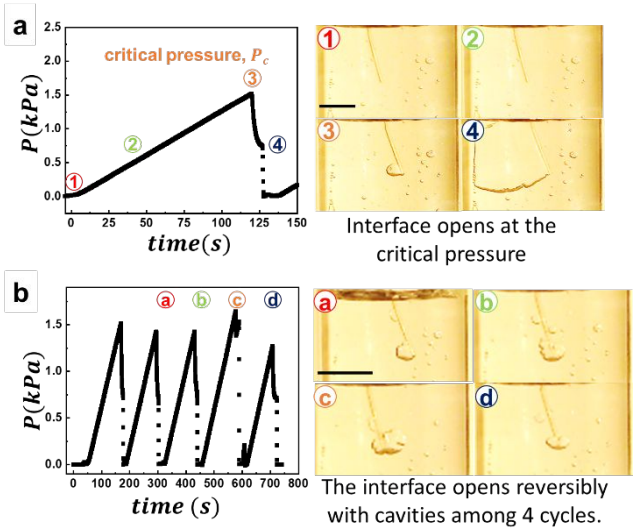

Figure 3. The pressure profile of needle-induced cavitation in ultra-soft interfaces. (a) A representative pressure profile with corresponding pictures. (b) Cyclic pressurization opens the ultra-soft hydrogel interface reversibly. Scale bar: 1cm.

3.3 Effect of residual stress

Determining the adhesion energy, or G_c, for the interface based on the measurement of the critical pressure requires the influence of the normal, residual stress to be eliminated. To investigate the residual stress effect on the critical pressure, we conducted interface-NIC measurements on hydrogel interfaces formed with PTFE sheets of thicknesses varying from 0.1 mm to 1.1 mm, using needles with outer diameters varying from 0.58 mm to 1.73 mm.

The finite element model provides the stress profile of the closed interface. It indicates that for a fully closed interface, the normal stress perpendicular to the interface has a symmetric distribution along the width direction of the interface, and the amplitude of the normal stress increases with the increase of thickness (Figure 2).

The critical pressures, normalized by hydrogel moduli, show that the critical pressure decreases linearly with increasing separator thickness for a given needle size, as shown in Figure 4(a). The slope of the decrease in critical pressure is approximately the same among the five needle sizes, as shown in Figure 4(b), suggesting that the linear decrease in critical pressure is only the result of separator thickness. By extrapolating the fitting curve to the y-axis, the intercept denoted as P_{c0}, is identified as the critical pressure when the separator thickness is zero. By subtracting P_c of a given separator thickness from P_{c0}, and dividing by the modulus, we obtain the normalized pressure difference, $\Delta P/E = (P_{c0} - P_c)/E$. We observe a linear relationship between $\Delta P/E$ and the normal stress at the same separator thickness, as shown in Figure 4(c). P_{c0} decreases with the increase of the needle size, as shown in Figure 4(d), suggesting that the needle size is

correlated to the initial crack size and that larger initial cracks can more easily satisfy the critical energy release rate criterion to initiate the crack, consistent with previous pressure-induced fracture theory and practice.[25–28]

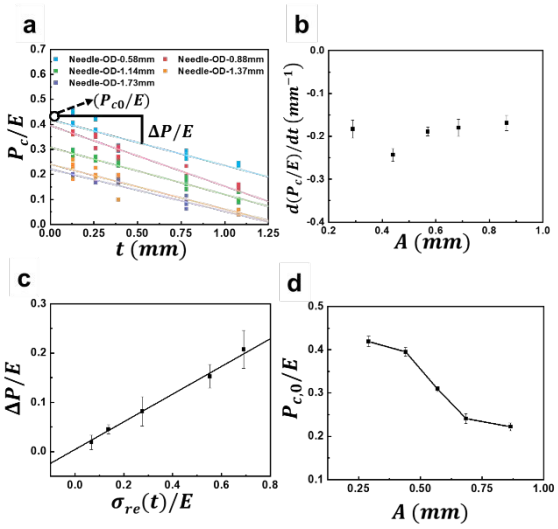

Figure 4. The critical pressure analysis. (a) The critical pressure dependence on the separator thicknesses and the needle radii.(b) The slopes of Pc versus t are independent of A for 4 out of 5 needle sizes. (c) The pressure decrease at given separator thicknesses versus the normal stress at the same separator thickness. (d) The critical pressure at zero thickness versus needle radii.

It is worth noting that the critical pressure of the interfacial failure is smaller than the critical pressure of regular NIC, which is determined to be $\frac{P_c}{\mu}=\frac{5}{2}+\frac{2\gamma}{\mu A}$. The pressure criterion of the interfacial failure is easier to achieve as compared with regular NIC, which is not surprising since the interface provides an initial weaker plane along which cavitation propagates.

3.4 Determining interfacial energy

We have obtained critical pressures to open the interface of hydrogels with various initial crack sizes defined by the needle radii. When we only consider the cross-section of the hydrogel sample, the tested region can be considered as a two-dimensional solid with an interface, as shown in Figure 4 (a1). As the needle is inserted, the hydrogel surface is deformed, and a void occurs in the center (Figure 4 (a2)), during which the contact elastic energy is stored. The hydrogel size is set by the size of the vial, while the void size varies depending on the needle outer diameter. The void expands elastically until the critical pressure is reached (Figure 4 (a3)), during which the potential energy of air and the resultant elastic energy of air pressure are stored. After the critical pressure is reached, the hydrogel-hydrogel interface is opened, and the new surfaces form by dissipating the total stored energy (Figure 4 (a4)). The general principle to calculate the interfacial energy is to account for the energy release rate G_c resulting from the sum of strain and potential energy, both of which decrease with crack initiation. The energy release rate (G) is given by the following equation:

$$G=\frac{d(U_e+U_p)}{dS}. \quad (1)$$

In Equation 1, U_e is the total strain energy stored in the solid, while U_p is the potential energy of air enclosed in the solid cylinder and the tube. U_e includes two sources: (1) deformation at the needle tip due to the inserted needle contacting to deform a closed interface, U_1 and (2) expansion in the axial direction under pressure, U_2, as shown in Figure 5(a). Therefore, strain energy is given by the expression as:

$$U_e=U_1+U_2 \quad (2)$$

Potential energy comes from the pressure applied to balance the axial expansion of the hydrogel, which is expressed by:

$$U_p=-PV_0 \quad (3)$$

In Equation3. P is the air pressure in the cylinder void and the tube, and V_0 is the toal air volume. We derive the algorithms of energy in the following section.

3.4.1 Contact strain energy by the needle insertion

During experiments, the PTFE needle is inserted into the closed hydrogel interface, which causes the needle to displace the initially contacting hydrogel surfaces. The hydrogel bulk deforms to accommodate the needle's outer edge, leading to the storage of the strain energy from contact (U_1). To estimate U_1, the configuration can be modeled as two half-spaces, with each half-space being contacted with a rigid half cylinder. The strain energy stored in each half-space is equal to the work (W) required to actuate the rigid cylinder to form a contacted width to be the same as the cylinder radius, where the cylinder radius in the model is the needle outer radius. Based on the contact mechanics of cylindrical bodies[29], the expression of U_1 can be obtained as:

$$U_1=2*W=2*\int_0^A F\,d\delta=K\mu A^2. \quad (4)$$

Here, μ is the shear modulus, A is the needle outer radius, δ is the rigid body displacement of the half cylinder, F is the resultant force of the rigid half cylinder contacting the solid, and K is a unitless geometry constant.

3.4.2 Pressure-induced strain energy and pressure balance

In addition to the contact strain energy determined by the radii of inserted needles, the strain energy is also governed by the elastic deformation initiated by the applied pressure. Also, the pressure balance relating to the deformation ratio in the azimuth direction can be derived. We analyze U_2 at the cross-section of the needle tip prior to the critical pressure with the internally-inflated cylinder model:

$$U_2=\int_A^{R_o\to\infty} u_2*\mathrm{d}(\pi R^2)=\frac{\pi}{2}\mu A^2(\lambda^2-1)\ln(\lambda^2). \quad (5)$$

Here, u_2 is the strain energy density, which is derived in Supplementary S3, R_0 is the outer radius of the solid, R is the

integral variable. $\lambda = a/A$ is the stretch ratio of the inner cylinder, and a is the radius of the inner cylinder at the deformed state, as shown in Figure 5(a). We assume that the internal radius is much smaller than R_0. In the experiments, the needle radius A is approximately 1 mm, while the hydrogel radius is about 15 mm. Thus, the assumption $A/R_0 << 1$ is validated.

The expression of the internal pressure with respect to the deformation is:

$$P = \frac{\mu}{2}\left(1 + \ln(\lambda^2) - \lambda^{-2}\right) + \frac{\gamma}{A}\lambda^{-1}. \quad (6)$$

Here, $\gamma = 0.07 J/m^2$ is the water surface tension. The elastic energy portion of Equation 6, $\frac{\mu}{2}\left(1 + \ln(\lambda^2) - \lambda^{-2}\right)$, has been reported previously[30], and Equation 6 also includes the non-negligible surface tension contribution to balancing the pressure for soft materials. The derivation of Equation 6 is shown in Supplementary S3. Substituting P_c into Equation 6 determines the critical stretch ratio at the inner cylinder, λ_c, which is the critical deformation at the inner cylinder when the critical pressure is reached.

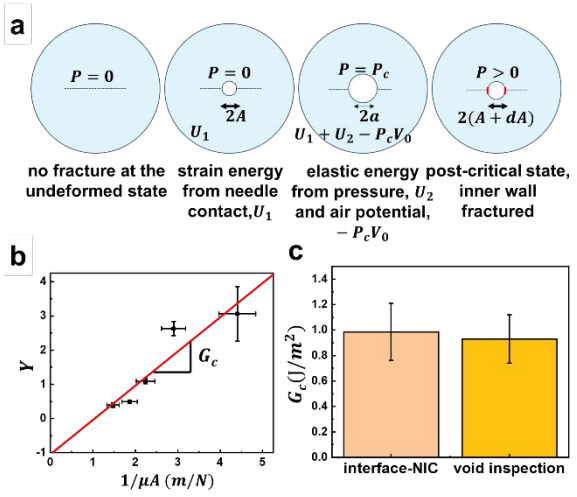

Figure 5. (a) A schematic of the 2D internal-inflated cylinder model from needle insertion to fracture under critical pressure. (b) The model prediction based on Equation 10. The slope of the fitting curve is G_c. The x-axis error bars are from the deviation of hydrogel moduli and y-axis error bars are from deviation of λ_c. (c) A cross-platform comparison of G_c results. The error bar of the pressurization method comes from the standard deviation of five Gc values with different needle radii.

3.4.3 Energy release rate

The total derivative of $U_e - PV_0$ is given by the following equation, consisting of the partial derivative of the strain energy and the potential energy with respect to the A and λ:

$$d(\mathrm{U}_e + U_p) = d(U_1 + U_2 - PV_0) = \left(\frac{\partial U_1}{\partial A}\right)_\lambda dA + \left(\frac{\partial U_1}{\partial \lambda}\right)_, \quad (7)$$

When we expand the expression of $d(\mathrm{U}_e + U_p)$, it becomes:

$$d(\mathrm{U}_e + U_p) = \left(\frac{\partial U_1}{\partial A}\right)_\lambda dA + \left(\frac{\partial U_1}{\partial \lambda}\right)_A d\lambda + \left(\frac{\partial U_2}{\partial A}\right)_\lambda dA + | \quad (7.1)$$

Previous studies utilized water as the intermediate in pressurization experiments or theoretical derivation and used the incompressibility of water to set the void volume as the boundary condition.[31–33] However, at the critical point of compressing air to initiate interface fracture, both the volume of the air and the pressure at the needle end change, which yields the simultaneous change of the initial size (equivalent to the needle outer radius A) and λ, respectively. We find the amount of air to be invariant, resulting in the boundary condition being $d(PV_0) = d\left(nR_{idealgas}T\right) = 0$. Here, n is the amount of air, $R_{idealgas}$ is the ideal gas constant, and T is the temperature, all of which are constant in the test. The constant quantity of air allows us to derive the relationship between dA and $d\lambda$, as:

$$d(PV_0) = \left(\frac{\partial PV_0}{\partial A}\right)_\lambda dA + \left(\frac{\partial PV_0}{\partial \lambda}\right)_A d\lambda = 0 \quad (8)$$

It should be emphasized that the most accurate expression of V_t includes the compressed volume ($-Qt$) in the air reservoir and the opened cylindrical void at the needle end ($\pi(A\lambda)^2 L_0$). Therefore, V_t should be expressed as $V_t = V_0 - Qt + \pi(A\lambda)^2 L_0$. In the experiment, V_0 (> 20000 μL) is much greater than Qt (~100 μL) and $\pi (A\lambda)^2 L_0$ (~1 μL). Therefore, we treat V_t to be a constant. By solving Equation 8, we obtain the relationship between dA and $d\lambda$. The ratio is defined to be $C = \frac{d\lambda}{dA} = -\frac{\left(\frac{\partial P}{\partial A}\right)_\lambda}{\left(\frac{\partial P}{\partial \lambda}\right)_A}$

$= \frac{\frac{\gamma}{\mu A}\lambda_c^2}{A\left(\lambda_c^2 + 1 - \frac{\gamma}{\mu A}\lambda_c\right)}$.

Additionally, U_1 is determined prior to the pressurization. It is independent of the stretch ratio. Therefore $\left(\frac{\partial U_1}{\partial \lambda}\right)_A = 0$. The derivative of undeformed area per unit length is given by $dS = 2\pi dA$. Consequently, the critical energy release rate expression is:

$$G_c = \left(\frac{\mathrm{d}(U_e - P_c V_0)}{dS}\right)_{P_c V_0} = \frac{\left(\frac{\partial U_1}{\partial A}\right)_\lambda dA + \left(\frac{\partial U_2}{\partial A}\right)_\lambda dA + (}{2\pi dA} \quad (9)$$

When we substitute all variables, the expression of G_c is:

$$G_c = \frac{1}{2}\mu A\left(\lambda_c^2 - 1\right) ln\, \lambda_c^2 + \frac{1}{2}\mu A^2(\lambda_c ln\, \lambda_c^2 + \lambda_c - \frac{1}{\lambda_c} \quad (9.1)$$

G_c and K are two unknown parameters. By rearranging Equation 9.1, we develop a linear equation that can be used to determine G_c and K:

$$\frac{1}{2}\left(\lambda_c^2 - 1\right)\ln \lambda_c^2 + \frac{1}{2}A(\lambda_c \ln \lambda_c^2 + \lambda_c - \frac{1}{\lambda_c})C = \frac{G_c}{\mu A} - \frac{K}{\pi}. \quad (10)$$

3.4.4 Calculation and validation of G_c

Plotting the left-hand side ($Y = \frac{1}{2}\left(\lambda_c^2 - 1\right)\ln \lambda_c^2 + \frac{1}{2}A(\lambda_c \ln \lambda_c^2 + \lambda_c - \frac{1}{\lambda_c})C$) provided in Equation 9.1 against $1/\mu A$ provides G_c from the slope and K/π from the intercept, as shown in Figure 5(b). We obtained G_c to be 0.99±0.22 J/m² and

K/π to be 1.02±0.63 when using the length unit as millimeter and the modulus unit as kPa. The data used for fitting can be found in Table S3 in Supplementary Information.

Due to the softness of the hydrogels, preparing samples for peel or tack tests to measure the hydrogel-hydrogel interfacial energy is problematic. In order to prepare hydrogel samples for peel or contact adhesion testing, the preparation conditions would need to be different to prevent diffused oxygen that would terminate the radical polymerization of the hydrogel. Therefore, a true comparison of interfacial properties would not be possible. We have discussed these differences with comparisons to contact adhesion testing of similar materials previously [21]. To validate the derived algorithm of the needle-induced cavitation test at interfaces, we apply the recently published "void inspection method" to compare the interfacial energy results[21]. The reason for using this method as a comparison is that the hydrogel specimens, and interfaces within, could be synthesized under similar conditions with respect to oxygen exposure. The void inspection method is used to determine the elasto-adhesion length scale. By measuring the hydrogel Young's moduli independently, we calculate G_c with a value of 0.93±0.19 J/m^2. Detailed information on the void inspection method can be found in Supplementary S4, Figure S1 and Table S2.

To assess the statistical significance of the difference between the two values, Welch's t-test is performed, assuming that the mean and standard deviation of the G_c values from both methods follow the normal distribution. The null hypothesis (H0) is that the difference between the mean values of G_c from the two methods is equal to zero ($\Delta = 0$), while the alternative hypothesis (H1) was that the two mean values of G_c were not equal ($\Delta \neq 0$). The calculated t-score is 0.438, and the resulting p-value is 0.680, which is larger than the significance level $\alpha = 0.05$. Therefore, we conclude that *there is not enough evidence to reject the hypothesis H0 at the significance level 0.05* (Figure 5(c)), thus validating the algorithm of the needle-induced cavitation at interfaces test.

Conclusions

In conclusion, we present a novel needle-based pressurization method for measuring the interfacial strength in ultra-soft hydrogels with residual stress. By manipulating the thickness of an inert PTFE separator inserted prior to the hydrogel polymerization, we create a hydrogel-hydrogel interface with varying normal stress and measure the critical pressure, which is the maximum pressure in the pressurization history, to open the interface. The critical pressure is influenced by the needle size and the residual stress. We determine the critical pressure in the absence of residual stress and convert this pressure to interfacial energy by calculating the energy release rate of the strain and potential energy, the former of which includes needle contact and internal inflation under pressure. Our experimental data validates that the derived algorithm is consistent with independently measured interfacial energy values obtained from another validated method. Our newly-introduced method offers the advantages of other needle-based methods, including the ability to apply this approach for studying the strength of interfaces *in vivo*. Moreover, our method is capable of quantifying the impact of residual stress on interfacial strength, making it especially useful for bio-based testing applications.

Author Contributions

Hongbo Fu, as the first author, is responsible for conceptualization, data acquisition, formal analysis, and original draft writing. Alfred Crosby, as the corresponding author, is responsible for validation, supervision, and review editing.

Conflicts of interest

The authors have no conflicts to declare.

Data Availability

The experimental data supporting the findings of this study were collected by the authors in the laboratory work and are available in the main text and Supplementary Information. The algorithms presented in the study were derived by the authors based on cited publications in the main text.

Acknowledgements

The authors acknowledge the support from the Office of Naval Research Grant (ONR N00014-17-1-2056)

Notes and references

1 J. A. Zimberlin, J. J. McManus and A. J. Crosby, *Soft Matter*, 2010, **6**, 3632–3635.

2 J. A. Zimberlin and A. J. Crosby, *J Polym Sci B Polym Phys*, 2010, **48**, 1423–1427.

3 J. A. Zimberlin, N. Sanabria-Delong, G. N. Tew and A. J. Crosby, *Soft Matter*, 2007, **3**, 763–767.

4 C. W. Barney, Y. Zheng, S. Wu, S. Cai and A. J. Crosby, *Soft Matter*, 2019, **15**, 7390–7397.

5 C. W. Barney, C. E. Dougan, K. R. McLeod, A. Kazemi-Moridani, Y. Zheng, Z. Ye, S. Tiwari, I. Sacligil, R. A. Riggleman, S. Cai, J. H. Lee, S. R. Peyton, G. N. Tew and A. J. Crosby, *Proc Natl Acad Sci U S A*, 2020, **117**, 9157–9165.

6 C. E. Dougan, H. Fu, A. J. Crosby and S. R. Peyton, *J Mech Behav Biomed Mater*, 2024, **160**, 106698.

7 S. Kundu and A. J. Crosby, *Soft Matter*, 2009, **5**, 3963.

8 C. E. Dougan, Z. Song, H. Fu, A. J. Crosby, S. Cai and S. R. Peyton, *Biophys J*, 2022, **121**, 2721–2729.

9 C. W. Barney, C. E. Dougan, K. R. McLeod, A. Kazemi-Moridani, Y. Zheng, Z. Ye, S. Tiwari, I. Sacligil, R. A. Riggleman, S. Cai, J. H. Lee, S. R. Peyton, G. N. Tew and A. J. Crosby, *Proc Natl Acad Sci U S A*, 2020, **117**, 9157–9165.

10 F. Ajalloueian, G. Lemon, J. Hilborn, I. S. Chronakis and M. Fossum, *Nat Rev Urol*, 2018, **15**, 155–174.

11 E. M. Boazak, J. d'Humières, A. T. Read and C. R. Ethier, *J Biomech*, 2019, **93**, 204–208.

12 R. H. Luo, N. K. Tram, A. M. Parekh, R. Puri, M. A. Reilly and K. E. Swindle-Reilly, *Curr Eye Res*, 2023, **48**, 195–207.

13 M. S. Jokandan, F. Ajalloueian, M. Edinger, P. R. Stubbe, S. Baldursdottir and I. S. Chronakis, *J Mech Behav Biomed Mater*, 2018, **79**, 92–103.

14 S. Sharma, A. Mandhani, S. Bose and B. Basu, *Acta Biomater*, 2021, **129**, 122–137.

15 N. F. Davis, J. J. E. Mulvihill, S. Mulay, E. M. Cunnane, D. M. Bolton and M. T. Walsh, *Urology*, 2018, **113**, 235–240.

16 C. E. Constantinou, M. S. Damaser and I. Perkash, *Ultrasound Med Biol*, 2002, **28**, 1157–1163.

17 C. E. Dougan, Z. Song, H. Fu, A. J. Crosby, S. Cai and S. R. Peyton, *Biophys J*, 2022, **121**, 2721–2729.

18 P. J. Flory, *Principles of polymer chemistry*, Cornell University Press, Ithaca, N.Y., 1953.

19 R. Marcombe, S. Cai, W. Hong, X. Zhao, Y. Lapusta and Z. Suo, *Soft Matter*, 2010, **6**, 784–793.

20 A. E. English, S. Mafé, J. A. Manzanares, X. Yu, A. Y. Grosberg and T. Tanaka, *Journal of Chemical Physics*, 1996, **104**, 8713–8720.

21 H. Fu and A. J. Crosby, *Soft Matter*, 2023, **19**, 932–937.

22 S. R. Polio, A. N. Kundu, C. E. Dougan, N. P. Birch, D. Ezra Aurian-Blajeni, J. D. Schiffman, A. J. Crosby and S. R. Peyton, *PLoS One*, , DOI:10.1371/journal.pone.0204765.

23 S. Rattan, L. Li, H. K. Lau, A. J. Crosby and K. L. Kiick, *Soft Matter*, 2018, **14**, 3478–3489.

24 H. K. Lau, S. Rattan, H. Fu, C. G. Garcia, D. M. Barber, K. L. Kiick and A. J. Crosby, *Macromol Biosci*, 2020, **20**, 1900360.

25 S. B. Hutchens, S. Fakhouri and A. J. Crosby, *Soft Matter*, 2016, **12**, 2557–2566.

26 S. Kundu and A. J. Crosby, *Soft Matter*, 2009, **5**, 3963.

27 J. Diani, *Int J Fract*, 2001, **112**, 151–161.

28 Y. Y. Lin and C. Y. Hui, *Int J Fract*, 2004, **126**, 205–221.

29 K. L. Johnson, *Contact Mechanics*, Cambridge University Press, Cambridge, 1985.

30 N. Cheewaruangroj, K. Leonavicius, S. Srinivas and J. S. Biggins, *Phys Rev Lett*, 2019, **122**, 2–3.

31 Y. Fu, T. Yin, S. Qu and W. Yang, *J Mech Phys Solids*, 2023, **172**, 105192.

32 A. N. Gent and C. Wang, *J Mater Sci*, 1991, **26**, 3392–3395.

33 J. Kang, C. Wang and S. Cai, *Soft Matter*, 2017, **13**, 6372–6376.

ARTICLE

zReceived 00th January 20xx,

Accepted 00th January 20xx

DOI: 10.1039/x0xx00000x

Measuring interfacial strength of ultra-soft materials with needle-induced cavitation

Hongbo Fu, [a] Alfred J. Crosby *[b]

Needle-induced cavitation (NIC) has been used to characterize the mechanical properties of ultra-soft biological tissues. Previous studies conducted NIC on brain tissue and computed the energy to separate, or fracture, interfaces between regions from the measured NIC critical pressure. These tests revealed the intrinsic correlation between the critical pressure and the interfacial properties. While NIC demonstrated its potential for measuring interfacial properties, independent measurements have not been made to validate the measurements. In this work, we use model interfaces to validate the use of NIC to quantify the interfacial energy of buried interfaces. By inserting a needle into the interface and inducing pressurized separation, we obtained the critical pressure dependence on the needle size and a known residual stress. At the extrapolated residual stress-free state, we obtained the interfacial energy (G_c) by considering energy dissipated in the separation initiation at the critical pressure point, yielding a G_c value that matches an independent measurement.

Data Availability

The experimental data supporting the findings of this study were collected by the authors in the laboratory work and are available in the main text and Supplementary Information. The algorithms presented in the study were derived by the authors based on cited publications in the main text.

[a.] *Address here.*
[b.] *Address here.*
[c.] *Address here.*
† Footnotes relating to the title and/or authors should appear here.
Electronic Supplementary Information (ESI) available: [details of any supplementary information available should be included here]. See DOI: 10.1039/x0xx00000x